COBEM-2017-2100
EXPERIMENTAL VALIDATION OF UNLOADING COMPLIANCE SOLUTIONS APPLICABLE TO C(T) AND SE(B) SPECIMENS

Gustavo Henrique Bolognesi Donato [1,2]
[1] gdonato@fei.edu.br
Régis de Matos Curvelo de Barros [2]
João Ferreira Júnior [2]
[2] Centro Universitário FEI, Humberto de Alencar Castelo Branco Av., 3972,
São Bernardo do Campo, SP, ZIP 09850-901

Abstract. *The design and maintenance of high performance structures demand structural integrity assessments considering the presence of flaws (cracks), which demands accurate properties regarding fatigue and fracture. These mechanical properties may be characterized, for example, through J-R or da/dN vs. ΔK curves. Such measurements are highly dependent on the instantaneous crack size during the experiments, which are commonly estimated through electrical, optical or unloading compliance techniques. Unloading compliance is based on the stiffness decrease caused by crack growth. In this scenario, this work focuses on the experimental validation of recent numerical unloading compliance solutions proposed by Donato and Moreira and, predicting instantaneous crack size on C(T) and SE(B) specimens incorporating three-dimensional effects. To achieve this, C(T) and SE(B) specimens were machined according to current standards (ASTM E1820 and ASTM E647) and tested in a universal testing machine MTS 810.25. Based on load-displacement records, normalized unloading compliance (μ) could be computed and instantaneous crack sizes (a) estimated through standards and recent numerical proposals. The predicted crack sizes were compared to real measurements. The results reveal that both solutions are accurate and provided deviations below ~ ±1.6% when compared to experiments. They are comparable for C(T) specimens but Donato and Moreira's proposals were slightly better for SE(B) geometries.*

Keywords: *Unloading compliance, experimental validation, ASTM compliance solutions, SE(B), C(T).*

1. INTRODUCTION

Understand how cracks behave in high toughness structural materials is a key subject for its use in high responsibility structures and components (API 579, 2016; BS 7910, 2013). This is of critical relevance for several fields such as aeronautical, oil & gas, nuclear and automotive as a result of the increasing demand for performance and efficiency (ANDERSON, 2017). The mechanical characterization of such materials is highly dependent on accurate resistance curves (*J-R* curves) and fatigue crack growth response (*da/dN vs. ΔK* curves), in order to predict and/or avoid failures caused respectively by ductile tearing followed by fracture or by fatigue crack growth. It is worth noting that both kinds of results correlate crack driving forces such as *K*, *J* and *CTOD* (whose calculations are recommended by, for example, ASTM E1820 (2016) and ASTM E647 (2015)) with instantaneous crack size *a*. Thus, measuring instantaneous crack size during fracture and fatigue tests is of paramount relevance for acquiring mechanical properties qualified to support life predictions and structural integrity evaluations. The crack size, a, can be estimated using optical, electric or elastic unloading compliance techniques; the last one is focused by this research, since is widely employed and rely upon the usually available transducers.

In simple terms, the elastic unloading compliance technique correlates instantaneous compliance (the inverse of specimen's stiffness) to the crack depth. Fig. (1) illustrates one *J-R* curve obtained by Joyce (1993) from a structural ferritic steel employing such method. It is evident that the driving force (in this case *J*-integral) is expressed as a function of crack length (*Δa*). However, the beginning of the curve shows a negative crack growth, which is not reasonable from a phenomenological point of view and possibly may be attributed rotation, closure, plasticity, among other effects that are beyond the scope of this study. The fact is that such occurrences motivated researchers (for example Vasudeven et al. (1994), Donato & Moreira (2013) and Moreira (2014)) to look for corrections and improved formulae applicable to the elastic unloading compliance technique.

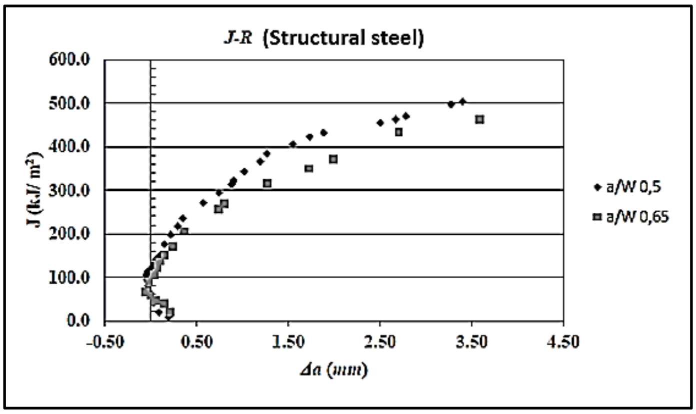

Figure 1. Example of spurious negative crack growth obtained in *J-R* testing of a ferritic steel (JOYCE, 1993).

In this context and considering the relevance of the correct measurement of instantaneous crack size for fatigue and fracture testing, the central objective of this work is to validate proposals found in the literature and developed by the research group for unloading compliance, which take into account 3-D effects and varying geometrical features. As a step in this direction, several C(T) and SE(B) samples were machined from an ASTM A516 gr. 70 steel and prepared under varying geometrical conditions for testing. Compliance was measured in detailed experiments and then compared to predictions from ASTM standards and other numerical proposals from the literature. The results proved that the evaluated available solutions are valid, but highlighted some benefits of employing some of them in specific cases.

2. THEORETHICAL BACKGROUND

2.1 Elastic unloading compliance method

The elastic unloading compliance technique correlates the increase of compliance *V/P* (or decrease of stiffness *P/V* – see Fig. 2(a)) with increasing crack size a. Fig. 2(b) indicates the main dimensions of SE(B) and C(T) specimens and *V* denotes the Crack Mouth Opening Displacement (CMOD). Since this method is based on load and displacement records that are usually acquired during fracture and fatigue testing, it does not demand any extra equipment other than a universal test machine and its transducers. In the case of *J-R* testing (ASTM E1820, 2016), the specimen is monotonically loaded and partially unloaded several times during crack extension (Fig. 3(a)). Load (*P*) is recorded *vs.* displacement (in terms of CMOD – *V* or LLD - *Δ*) during the whole test (in this work, *V* is used). Elastic and plastic areas (A_{pl} and A_{el}) are the basis for calculating instantaneous crack-driving forces. In each unloading, the stiffness (*1/C*) can be computed based on *P-V* data and reflects crack size at that moment. Testing standards provide polynomial expressions that relate instantaneous *a/W* to the experimental compliance *C*, as will be presented next. In the case of cyclic loading (*FCG* – Fig. 3(b)), the hysteresis loop allows to determine the value of compliance *C*, as showed in Fig 3(b).

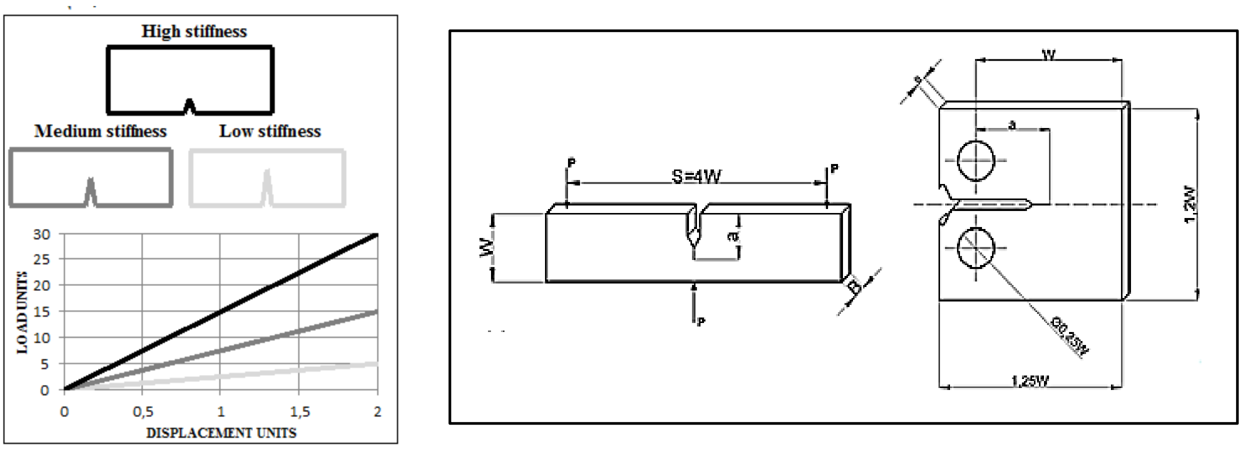

(a) (b)

Figure 2. (a) Fundamental of the unloading compliance technique and (b) basic geometry of SE(B) (left) and C(T) (right) specimens.

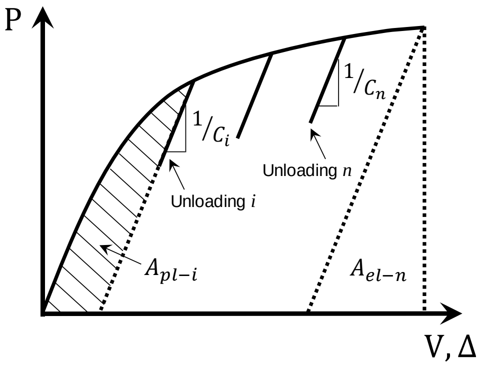

(a)

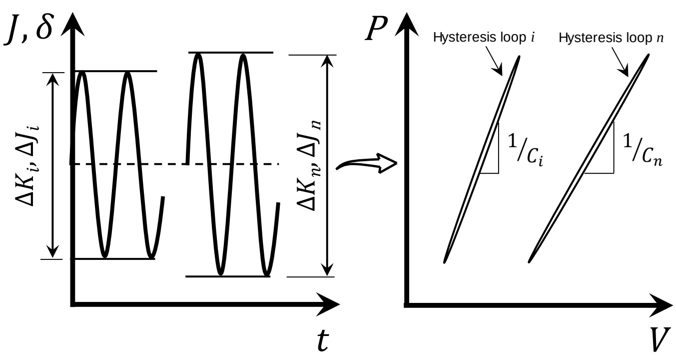

(b)

Figure 3. (a) Load-displacement curve from *J-R* testing including partial unloadings and different instantaneous compliances *C* and (b) Cyclic loading under load control (fixed *P*) leading to fatigue crack growth and therefore increasing *ΔK*, *ΔJ* and *C*.

As a general law, compliance is represented by Eq. (1). However, in order to make compliance independent on dimensions and materials, normalized versions are presented by Eqs. (2-3) respectively for C(T) and SE(B) specimens (CLARKE, 1976; ASTM E1820, 2016)

$$C = \frac{V}{P} \tag{1}$$

$$\mu = \frac{1}{1 + \sqrt{B_{eff}.E.C}} \tag{2}$$

$$\mu = \frac{1}{1 + \sqrt{\frac{B_{eff}.E.C.W}{\frac{S}{4}}}} \tag{3}$$

The dimensions *B* and *W* are showed by Fig. 2(b) and further details and definitions (like effective thickness - B_{eff}) can be found in ASTM E1820 (2016). The most important aspect of such normalized compliances is that they are obtained from experiments and, in thesis, are directly related to instantaneous crack sizes. Consequently, a key-issue is to have available solutions that correlate μ with the respective crack size (*a/W*) in the specimen being tested. Usually, polynomial equations that relate the crack size with normalized compliance are available, as presented next.

2.2 Revision of available compliance solutions applicable to C(T) and SE(B) samples

After an extensive literature review, it was found that current standardized equations (ASTM E1820 (2016), ASTM E647 (2015)) are based on the studies of Saxena & Hudak (1978), with improvements in its coefficients, derived from the work of Clarke et. al. (1976) and Joyce & Gudas (1979), for C(T) specimens. For SE(B) specimens, the literature review revealed that the solutions are based on the works of Joyce & Hackett (1992) and Wu (1984). Eq. (4) describes the general fiftieth grade polynomial equation applicable to unloading compliance method, while Table 1 presents the recommended coefficients from ASTM and considered by the authors as nowadays active in such standards.

$$\frac{a}{w} = \beta_0 + \beta_1\mu^2 + \beta_2\mu^2 + \beta_3\mu^3 + \beta_4\mu^4 + \beta_5\mu^5 \tag{4}$$

Table 1 – Coefficients of the polynomial solution for Eq. (4).

Specimen	$\boldsymbol{\beta_0}$	$\boldsymbol{\beta_1}$	$\boldsymbol{\beta_2}$	$\boldsymbol{\beta_3}$	$\boldsymbol{\beta_4}$	$\boldsymbol{\beta_5}$
SE(B) – 0.05≤*a/W*≤0.45	0.9997	-3.950	2.9821	-3.214	51.515	-113.0
SE(B) – 0.30≤*a/W*≤1.00	1.0188	-4.537	9.010	-27.33	74.40	-71.49
C(T) – 0.20≤*a/W*≤0.975	1.0002	-4.063	11.64	-106.0	464.33	-650.7

Despite active, the aforementioned solutions are in most cases the result of 2-D FE models and do not incorporate several relevant effects, such as rotation effects (caused by large deflections), contacts, closure, 3-D effects, plasticity in the vicinity of the crack, among others. Focusing on 3-D effects, which includes thickness and side-grooves, Donato & Moreira (2013) and Moreira (2014) showed that current solutions for SE(B) geometry may lead to deviations around 6% in some cases of crack size estimation. In other cases, such authors reveal errors larger than 10%, in special for shallow cracks. Such inaccuracies can compromise the quality of results and thus the safety of real structural integrity assessments.

2.3 Compliance solutions considering 3-D effects

Shen et al. (2010, 2012) studied the 3-D effects on compliance solutions applicable to SE(B) and SE(T) specimens with the aid of finite elements models. In addition, Wang & Zhou (2012) performed additional studies regarding SE(B) specimens. After that, Donato & Moreira (2013) and Moreira (2014) performed a comprehensive numerical study including C(T), SE(B) and SE(T) specimens under a wide variety of conditions. The developed FE models considered 3-D effects and are illustrated by Fig. 4 since different thicknesses and side-grooves were investigated by such authors. Eqs. (5-7) were proposed by them for C(T) specimens, while Eqs. (8-10) for SE(B) specimens. Each formulation is valid for one *W/B* ratio, which means 3-D effects are included. The numerical studies conducted by the same authors revealed a better crack size prediction when compared to solutions from literature and standards. However, experimental validations were missing and this work represents one step in this direction, based on preliminary experimental results.

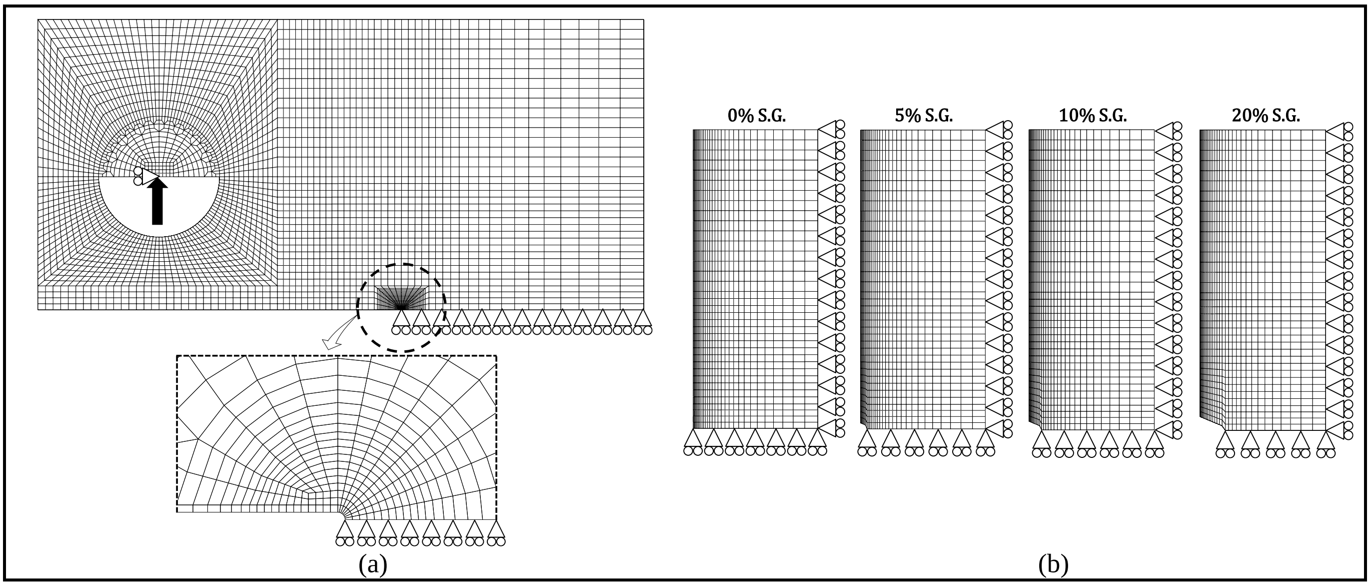

Figure 4 – (a) Quarter-symmetric finite element model used for a C(T) fracture specimens with *a/W* = 0.5. All other models present very similar features. (b) Different side-groove depths applied to C(T) FE models (DONATO & MOREIRA, 2013).

$$\frac{a}{w} = 0.91824 - 1.12547.(\mu) - 28.3229.(\mu^2) + 150.99949.(\mu^3) - 326.649.(\mu^4) + 277.2825.(\mu^5)$$
$$\left(\mathrm{C(T)};\ \mathrm{W} = 4\mathrm{B};\ 0.1 \le \frac{\mathrm{a}}{\mathrm{W}} \le 0.7\right) \tag{5}$$

$$\frac{a}{w} = 0.92388 - 1.30496.(\mu) - 25.81199.(\mu^2) + 134.687.(\mu^3) - 277.5005.(\mu^4) + 222.36279.(\mu^5)$$
$$\left(\mathrm{C(T)};\ \mathrm{W} = \mathrm{B};\ 0.1 \le \frac{\mathrm{a}}{\mathrm{W}} \le 0.7\right) \tag{6}$$

$$\frac{a}{w} = 0.92111 - 1.37650.(\mu) - 23.21792.(\mu^2) + 113.3446.(\mu^3) - 208.6299.(\mu^4) + 144.31037.(\mu^5)$$
$$\left(\mathrm{C(T)};\ \mathrm{W} = \mathrm{B};\ 0.1 \le \frac{\mathrm{a}}{\mathrm{W}} \le 0.7\right) \tag{7}$$

$$\frac{a}{w} = 0.98754 - 3.52941.(\mu) - 1.40431(\mu^2) + 21.06857.(\mu^3) - 31.77900.(\mu^4) + 18.94740.(\mu^5)$$

$$\left(\mathrm{SE(B)};\ \mathrm{W} = 4\mathrm{B};\ 0.1\ \leq \frac{\mathrm{a}}{\mathrm{W}} \leq\ 0.7\right) \tag{8}$$

$$\frac{a}{w} = 0.98543 - 3.45698.(\mu) - 1.89955.(\mu^2) + 21.22081.(\mu^3) - 24.84440.(\mu^4) + 5.50667.(\mu^5)$$

$$\left(\mathrm{SE(B)};\ \mathrm{W} = 2\mathrm{B};\ 0.1\ \leq \frac{\mathrm{a}}{\mathrm{W}} \leq\ 0.7\right) \tag{9}$$

$$\frac{a}{w} = 0.98228 - 3.55580.(\mu) - 1.37261.(\mu^2) - 5.00853.(\mu^3) + 60.18464.(\mu^4) - 91.6739.(\mu^5)$$

$$\left(\mathrm{SE(B)};\ \mathrm{W} = \mathrm{B};\ 0.1\ \leq \frac{\mathrm{a}}{\mathrm{W}} \leq\ 0.7\right) \tag{10}$$

3. EXPERIMENTAL PROCEDURES

The selected material for the study was an ASTM A516 gr. 70 steel obtained as hot rolled plates. The monotonic mechanical properties of the material were quantified by Ganharul (2012) and are presented by Table 2. The chemical composition was evaluated by the authors and is presented by Table 3. Forty eight specimens were machined (24 C(T) and 24 SE(B), considering 3 thicknesses (in terms of the *W/B* ratios = 1; 2; 4) and 3 crack depths (*a/W = 0.2; 0.5*; *0.7*). Figures 5(a-c) presents the details. The notches and respective knife edges were implemented using EDM machining and all specimens were measured using profile projector before and after testing (Fig. 5(d)).

Table 2 – Mechanical properties of the studied ASTM A516-Gr70.

Material	E (MPa)	σ_{ys} (MPa)	σ_{uts} (MPa)	H (MPa)	n ( )
ASTM A516	202	286.5	764.5	964.5	0.2372

Table 3 – Chemical composition ASTM A516-Gr70.

Material	C (%)	Mn (%)	Si (%)	Al (%)	P (%)	S (%)
ASTM A516	0.2	1.05	0.32	0.04	0.015	0.008

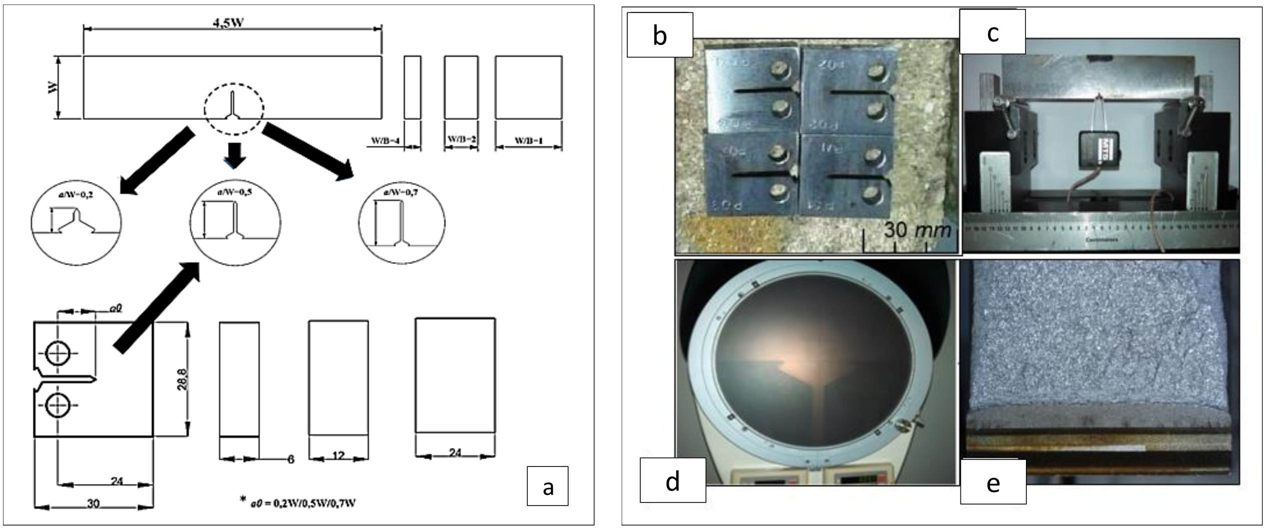

Figure 5 – (a) Final dimensions of the machined specimens, (b-c) C(T) and SE(B) specimens ready for testing, (d) specimens being measured and (e) post-mortem analysis of crack real depth.

Notch sizes resulting in relative depths (*a/W*) of ~ 0.2, 0.5 and 0.7 were achieved. To assess the experimental elastic unloading compliance, the following procedure was implemented (Figure 6):

- Load the specimen up to 10% of $K_{máx}$ (for this material, it means 18 MPa.m^{0,5}).
- Employed load rate: 10N/s.
- Unload until zero.
- Collect raw CMOD (*V*) and load (*P*) data, in order to evaluate compliance and correct for closure if necessary.

It is worth mentioning that a 2 kN load cell was properly calibrated using a certified reference load cell and used between 10% and 90% of its maximum range. In addition, an MTS clip-gage with 3 mm travel was calibrated using MTS micrometric drum before CMOD measurements. During the experiments, each specimen was loaded and unloaded 3 times following the aforementioned procedures.

In order to generate a refined data post-processing, the raw *P-V* records were analyzed in a MatLab algorithm specially developed by the authors for this research. Nonlinearities were filtered, closure events identified and only the linear loading-unloading regimes were taken into account for compliance computations. Each experimental compliance (*C* – Eq. (1)) was an average of the multiple loadings/unloadings, replicated specimens and, based on that, the algorithm could calculate the normalized compliance (μ) and its correlation to the size of the real machined notch (*a/W*).

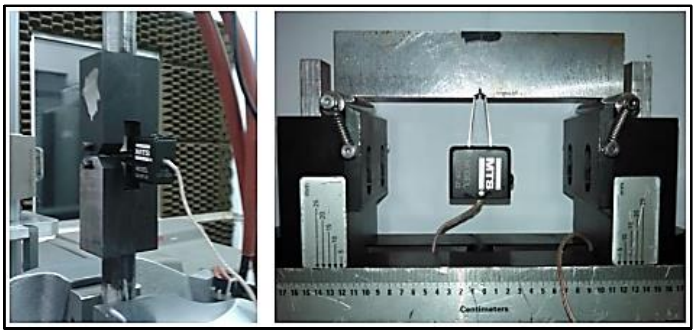

Figure 6 – (a) Testing apparatus for C(T) and SE(B) specimens.

After quantifying compliances for the notched condition (which is the focus of present paper), all specimens were pre-cracked under a frequency of 10 Hz and a load corresponding to $K_{máx}$, as suggested by ASTM E1820 (2016). All samples were then heat-tinted, using a 300ºC exposure for ~ 30 minutes. Compliance measurements were repeated for the pre-cracked condition using the same approach, but such measurements are out of the scope of this paper since are under post-processing. Finally, the pieces were fractured, to make possible the observation of the real notch and crack sizes. Images were acquired using a stereoscopic magnifier and measurements were conducted in a specific computer program developed by the research group (Fig. (7)). The *a/W* equivalent values were defined using the ASTM 9-point approach (ASTM E399 (2012)) and standard limits were considered for validating or invalidating samples.

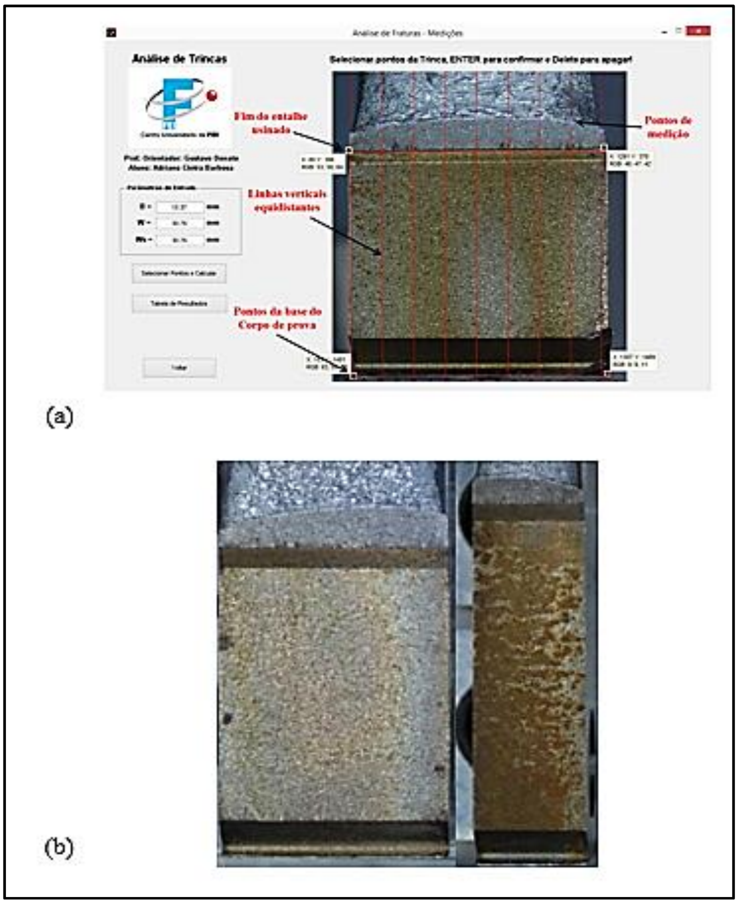

Figure 7 – Software developed at FEI's Structural Integrity, Fatigue and Fracture group for crack size measurements.

4. RESULTS AND DISCUSSION

The first result gathered with the tests is related to the feasibility of testing shallow-cracked C(T) specimens. In special for low *W/B* ratios (large thickness), such crack sizes (up to *a/W* ~ 0.2) lead to very stiff specimens where tensile loading is as severe as bending. It causes intense localized plastic deformation around the loading pins and remarkable friction effects. Consequently, such samples were discarded and its use for real testing is not recommended, since many assumptions are violated. For C(T) containing medium (*a/W* ~ 0.5) and deep defects (*a/W* ~ 0.7) and all SE(B) cases, all tests were perfectly feasible and with representative results. Figs. (8-9) present the relative agreement between measured crack sizes and those predicted (using solutions from ASTM E1820 (2016), Donato & Moreira (2013) and Moreira (2014) – the last two sources come from the same research group).

The assessment of Figs. (8-9) reveal that, for C(T) specimens, both solutions provided deviations under ~ ± 1%, which means both proposals are acceptable and will provide good crack size estimations. Except from the case where *W = 4B* and *a/W ~0.5*, all other situations presented low standard deviations, under ~ ± 2%. However, the standard deviations is high if compared to the average deviations due to the small number of specimens in the sample; despite in all cases the proposals of Donato & Moreira presented less standard deviation, as overlapping on this quantity occurred, no discrimination between the quality of the compliance solutions can be formally discussed. Finally, it is worth noting that no remarkable trend or effect of *W/B* or crack depth could be identified in the obtained deviations.

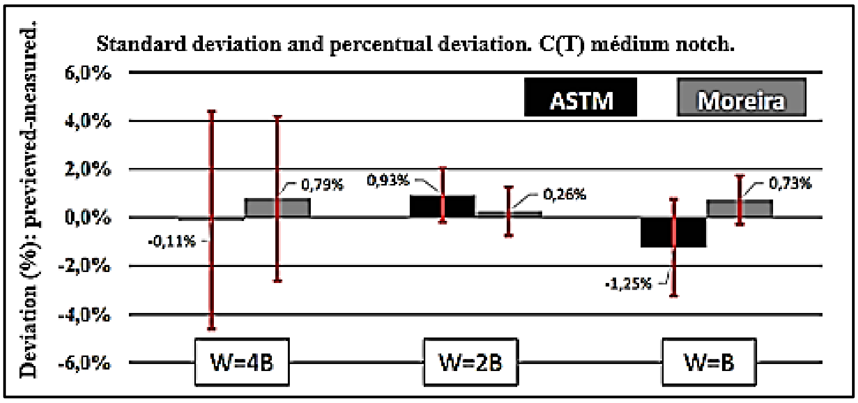

Figure 8 – C(T) results. Medium depth notch (*a/W* ~ 0.5).

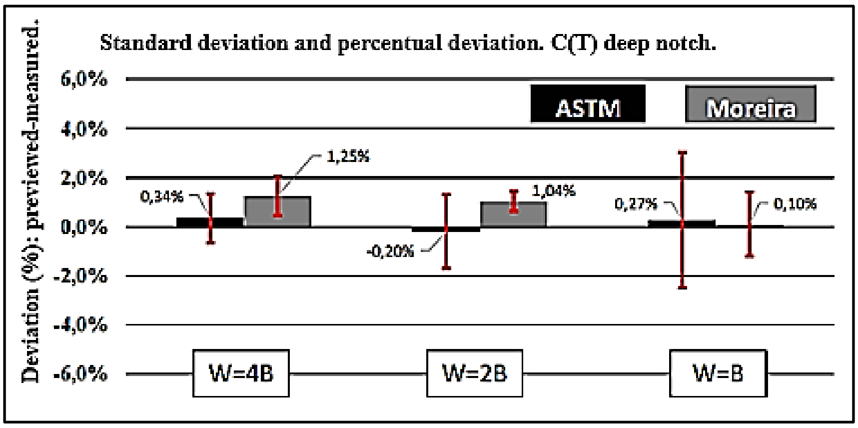

Figure 9 – C(T) results. Deep notch (*a/W* ~ 0.7).

Considering SE(B) specimens, all notch depths and thicknesses could be successfully tested and no issues regarding loading, alignment or anomalous deformation of the specimen were identified. The results, analogous to the ones presented for C(T), are presented for SE(B) geometries by Figs. (10-12) respectively for shallow, medium and deep notches.

In terms of the crack size predictions, one can realize that, considering average values, ASTM predictions are under ± 2% deviation in all cases, while Donato & Moreira's predictions are in all cases below ± 1%, being most cases below ± 0.5%. In average terms, thus, occurred a systematic increase in the quality of predictions including 3-D effects. However, the overlapping of some standard deviations does not allow to consider this result statistically robust. From a phenomenological point of view, on the other hand, the better average performance when compared to C(T) specimens was expected, since SE(B) geometry presents less difficulties regarding contacts, indentation and friction in loading rollers, and all effects could be incorporated and corrected by the refined 3-D models developed by Donato & Moreira (2013) and Moreira (2014).

Considering the scenario, similarly to C(T) specimens, the results obtained for SE(B) allow one to consider both solutions from ASTM and Donato & Moreira as validated for SE(B) geometries. However, taking into account the possible benefits, the sequence of studies with a larger number of samples is highly recommended looking for lower standard deviations associated with the results and its statistical relevance.

It should also be mentioned that normality tests (Shapiro-Wilk and t-test - both performed with the aid of a specific routine in MatLab) confirmed that the crack size follows a normal distribution.

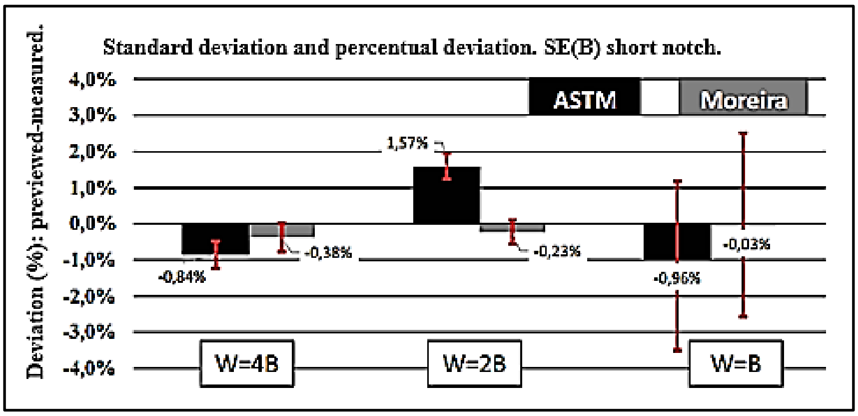

Figure 10 – SE(B) results. Shallow notch (*a/W* ~ 0.2).

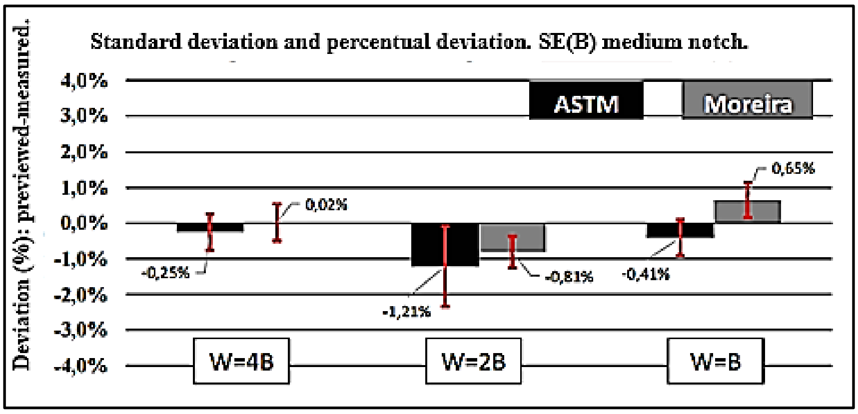

Figure 11 – SE(B) results. Medium depth notch (*a/W* ~ 0.5).

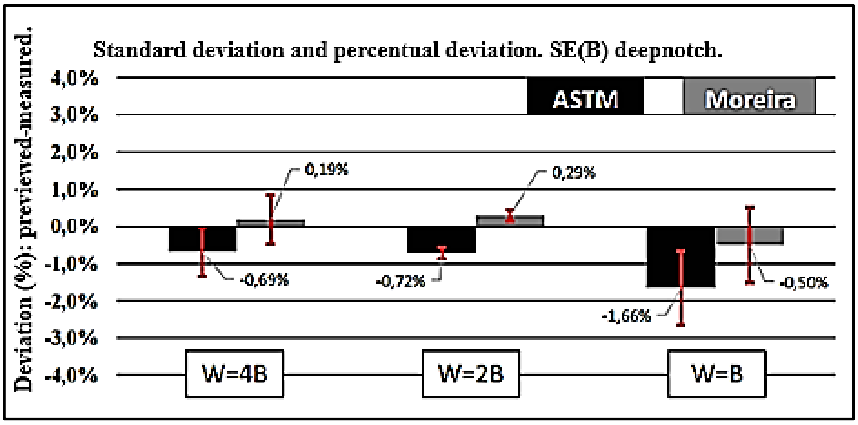

Figure 12 – SE(B) results. Deep notch (*a/W* ~ 0.7).

5. CONCLUDING REMARKS

From the obtained results, the following conclusions can be addressed:

Testing C(T) specimens with short crack-like defects ($a/W \sim 0.2$) is not recommended, since high loads induce local deformation around the loading holes and high friction, providing spurious crack size estimations.

In C(T) samples, was not evidenced the effect of *W/B* on the accuracy of crack size predictions using elastic unloading compliance. In addition, both solution sets provided deviations under ~ ± 1%, which means both proposals (ASTM and Donato & Moreira) are statistically comparable and will provide good crack size estimations. Despite the proposals of Donato & Moreira have presented lower standard deviation, some overlappings occurred in this quantity and a larger set of samples is recommended to have robust conclusions.

Considering SE(B) specimens, all notch depths and thicknesses could be successfully tested, and it is interesting to mention the enhanced control stability in the testing machine if compared to C(T) specimens, in which friction plays a larger role.

In terms of the crack size predictions for SE(B) geometry, considering average values, ASTM predictions are under ± 2% deviation in all cases, while Donato & Moreira's predictions are in all cases below ± 1%, being most cases below ± 0.5%. However, again some overlappings of the standard deviations were found and additional specimens in the samples are recommended.

Overall, even with the aforementioned overlaps on some standard deviations, there is a clear trend of better performance of the solutions proposed by Donato & Moreira when average deviations are evaluated for SE(B) specimens. For C(T) specimens, both solutions are considered comparable.

The obtained results increase the knowledge about the applicability and limitations of the numerical solutions for unloading compliance technique applicable to C(T) and SE(B) specimens.

6. ACKNOWLEDGEMENTS

This investigation is supported by the Brazilian Council for Scientific and Technological Development - CNPQ (grant 486176/2013-4), by the Coordination for the Improvement of Higher Education Personnel - CAPES and by Centro Universitário FEI, Brazil, through the use of its laboratories and human resources.

7. REFERENCES

Anderson, T. L., *Fracture Mechanics: Fundamentals and Applications* – 4rd edition, CRC Press, New York, 2017.

American Petroleum Institute - API, "Fitness-For-Service", API 579-1 / ASME FFS-1, 3rd ed., 2016.

American Society for Testing and Materials - ASTM. "Standard Test Method for Measurement of Fracture Toughness", ASTM E 1820, Philadelphia, 2016.

American Society for Testing and Materials - ASTM, "Standard Test Method for Linear-Elastic Plane-Strain Fracture Toughness K_{IC} of Metallic Materials", *ASTM E 399*, Philadelphia, 2012.

American Society for Testing and Materials - ASTM. "Standard Test Method for Measurement of Fatigue Crack Growth Rates", ASTM E 647, Philadelphia, 2015.

British Stantards Institute - BSI, "Guide to methods for assessing the acceptability of flaws in metallic structures", BS 7910:2013 + A1:2015, 2013.

Clarke, G. A. "Single specimen tests for J_{IC} determination". Mechanics of Crack Growth, ASTM STP 590, p. 27-42, Philadelphia, 1976.

Donato, G. H. B., Moreira, F. C., "Effects of side-grooves and 3-D geometries on compliance solutions and crack size estimations applicable to C(T), SE(B) and clampled SE(T) specimens", proc. of ASME PVP 2013, 2013.

Ganharul, G. K. Q. "Avaliação fenomenológico-experimental do efeito da triaxialidade de tensões pós-instabilidade na determinação das propriedades tensão-deformação por meio do ensaio de tração uniaxial". Dissertação de mestrado - Centro Universitário FEI, São Bernardo do Campo, 2012.

Joyce J. A.; Hackett, E. M. "Comparison of J_{IC} and *J-R* curves for short crack and tensilely loaded specimen geometries of a high strength structural steel". NUREG/CR-5879, US Nuclear Regulatory Commission, Washington, DC, 1992.

Joyce J. A.; Hackett, E. M.; Roe, C. "Effects of crack depth and mode of loading on the J-R curve behavior of a high strength steel". ASTM STP 1171: Elastic-Plastic Fracture. Philadelphia, p. 451-468, 1993.

Joyce, J. A.; Gudas, J. P. Computer interactive J_{IC} testing of navy alloys. ASTM STP 668: Elastic-Plastic Fracture. Philadelphia, p. 451-468, 1979.

Moreira, F. C. "Determinação numérica de limites de deformação e flexibilidades elásticas aplicáveis a geometrias C(T), SE(B) e SE(T)". Dissertação de mestrado - Centro Universitário FEI, São Bernardo do Campo, 2014.

Vasudeven, A. K.; Sandananda, K.; Louat, N. "A review of crack closure, crack threshold and related phenomena". Materials science and engineering, V. 2, p. 1-22, 1994.

Saxena, A.; Hudak Jr.; S. J. "Review and extension of compliance information for common crack growth specimens", Int. Journal of Fracture, V. 14, Issue 5, pp. 453-468, 1978.

Shen, G., Tyson, W. R., Gianetto, J. A., Park, D., "Effect of Side Grooves on Compliance, J-integral and Constraint of a Clamped SE(T) Specimen", Proc. of ASME PVP 2010, 2010.

Shen, G., Tyson, W. R., Gianetto, J. A., "CMOD Compliance of BxB Single Edge Bend Specimens", Proc. of ASME PVP 2012, 2012.

Wang, E., Zhou, W., "A Numerical Study on CMOD Compliance for Single-Edge Bending Specimens", proc. of ASME PVP 2012, 2012.

Wu, S. "Crack length calculation formula for three point bend specimens". International Journal of Fracture, p. 33-38, 1984.

8. RESPONSIBILITY NOTICE

The authors are the only responsible for the printed material included in this paper.